BNL-94620-2011-JA

SPECTRAL SOLAR IRRADIANCE AND ITS ENTROPIC EFFECT ON EARTH'S CLIMATE

Wei Wu[1], Yangang Liu[1], and Guoyong Wen[2,3]

[1]Atmospheric Sciences Division, Brookhaven National Laboratory, Upton, NY 11973
[2]NASA Goddard Space Flight Center, Greenbelt, MD
[3]Goddard Earth Sciences and Technology Center, University of Maryland, Baltimore, MD

Submission for publication in *Journal of Atmospheric Science*
July 2011

Atmospheric Sciences Division/Environmental Sciences Dept.

Brookhaven National Laboratory

U.S. Department of Energy
Office of Science

DISCLAIMER

Abstract

The high-resolution measurements of the spectral solar irradiance (SSI) at the top of the Earth's atmosphere by the Solar Radiation and Climate Experiment (SORCE) satellite are used to examine the magnitude and spectral distribution of the Earth's entropy flux from the TOA incident solar radiation. Two extreme cases are examined by using Planck expression: I. isotropic hemispheric incident solar radiation; II. (a) the specific energy intensity of solar radiation received at the top of the atmosphere (TOA) is the same as that radiated at the Sun's surface, and (b) incident solar radiation is isotropic within the cone of the solid angle to the Sun subtended by any point at the TOA. The estimated Earth's entropy flux from the observed SSI under the assumption I is shown about 4 times larger than that under the assumption II. The difference in magnitude is comparable to the typical value of the entropy production rate associated with atmospheric latent heat process. Further comparison with a conventional approach by using a blackbody Sun's brightness temperature exhibits that the estimated Earth's entropy flux from a blackbody Sun under the assumption II is about the same as that from the conventional approach. Furthermore, sensitivity study shows that the variability of TOA SSI could significantly impact the magnitude and spectral distribution of the estimated Earth's entropy flux. Overall, this study suggests that the measurements of the TOA SSI are crucial for estimating the entropy production rate of the Earth's climate.

1. Introduction

Modern satellite observations have demonstrated that although the total solar irradiance (TSI) at the top of the Earth's atmosphere (TOA) varies little (only about 0.1%), the Sun is a highly variable star with a substantial variation of TOA spectral solar irradiance (SSI) (Harder et al. 2009). Because solar radiation is the primary driving force for all the activities within the Earth's climate and radiation at different wavelengths reaches and warms different atmospheric layers, this finding raises some important questions critical to studying the Earth's climate: What is the consequence of the changing TOA SSI to the Earth's climate? Could this finding change our view of greenhouse-gas induced global climate change?

Based on the daily observations of the solar spectrum between 200 nm and 2400 nm from the Spectral Irradiance Monitor (SIM) instrument on the Solar Radiation and Climate Experiment (SORCE) satellite, Harder et al. (2009) found that the primary contributors to TSI (i.e., irradiance at ultraviolet, visible, and near infrared wavelengths) exhibit significantly different variability with time. The irradiance at ultraviolet (200 nm to 400 nm) wavelengths shows a significant decline from April 2004 to February 2008 while the irradiance at visible (400 nm to 691 nm) or the near infrared (972 nm to 2423 nm) wavelengths shows a large increase and the irradiance at the near infrared (691 nm to 972 nm) wavelengths shows a small decrease (see Figure 3 in Harder et al., 2009). It has been known that radiation at ultraviolet wavelengths mainly heats stratosphere and is critical to producing stratospheric ozone, and radiation at visible and near infrared wavelengths mainly heats troposphere as well as the Earth's surface. Thus, the significantly different variability of the primary contributors to TSI is intuitively expected to have a large impact on the vertical profiles of atmospheric ozone and temperature as well as the Earth's surface temperature.

A series of recent papers has investigated the Earth's climate responses to the TOA SSI variability as reported by Harder et al. (2009), suggesting that the impacts of the TOA SSI variability on the Earth's climate could be significantly different from our current understanding, especially on the vertical profiles of atmospheric ozone and temperature (e.g., Cahanlan et al., 2010; Haigh et al., 2010). For example, Cahanlan et al. (2010) used the findings by Harder et al. (2010) to construct two 11-year sinusoidal scenarios of TOA SSI forcing with the same TSI. One has out-of-phase SSI variability as in the SIM-based observations and the other has in-phase SSI variability as the reconstructed solar radiation from a widely used solar radiation reconstruction

model by Lean (2000). Then, they used the two scenarios of TOA SSI forcing to drive a radiative-convective model and a global climate model (i.e., Goddard Institute for Space Studies modelE of National Aeronautics and Space Administration) to investigate the difference of the Earth's climate responses. They found that the two scenarios lead to significantly different climate responses, especially in upper stratosphere where temperature response to the out-of-phase scenario shows 5 times larger than that to the in-phase scenario. Additionally, Haigh et al. (2010) employed a radiative photochemical model to investigate the impact of the SIM-based out-of-phase TOA SSI variability on stratosphere by comparing with the Lean-model reconstructed in-phase TOA SSI variability. They found that the SIM-based out-of-phase TOA SSI variability could lead to a significant decline in stratospheric ozone below an altitude of 45 km from 2004 to 2007 and an increase above this altitude. Besides, they also found that according to the SIM-based TOA SSI observations the tropopause SSI has an increase over the declining phase of solar cycle 23 (i.e., out-of-phase with declining solar activity from 2004 to 2007), which is opposite to our previous understanding. Furthermore, Gray et al. (2010) reviewed current understanding of the influence of solar variability on the Earth's climate from solar variability, solar-terrestrial interactions and the mechanisms determining the response of the Earth's climate. They emphasized that if the out-of-phase TOA SSI variability in the SIM-based observations is real, responses in both stratospheric ozone and temperature are expected to be much different from current expectations as indicated by Haigh et al. (2010) and thus need to be reassessed. They suggested a need of further observations and research for improving our understanding of solar forcing mechanisms and their impacts on the Earth's climate, including understanding the SIM-based out-of-phase TOA SSI variability and assessing their influence on the Earth's climate.

Here, we are motivated to investigate entropic impact of the SIM-based out-of-phase TOA SSI variability on the Earth's climate by using the SIM-based SSI observations to examine the magnitude and spectral distribution of the Earth's entropy flux from the TOA incident solar radiation. Entropy, as a fundamental thermodynamic quantity additional to temperature and energy, has been shown critical for studying the Earth's climate (e.g., Pujol and Fort, 2002; Ozawa et al., 2001; Paltridge et al., 2007; Pauluis et al., 2002a, b; Wang et al., 2008; Jupp and Cox, 2010; Lorenz, 2010; Wu and Liu, 2010b; Liu et al., 2011; Lucarini and Ragone, 2011). A broad range of entropy applications on the Earth's biosphere-atmosphere system including

aspects such as atmospheric circulation, role of clouds, hydrology, ecosystem exchange of energy and mass can be found in a special issue published in Philosophical Transactions of the Royal Society B (Kleidon et al., 2010). The radiation exchange between the Earth's climate and its surrounding space provides us thermodynamic constraints not only from energy conservation dictated by the first law of thermodynamics but also from entropy production rate associated with the second law of thermodynamics. It is anticipated that integration of this entropy-related thermodynamic constraint into current global climate models could improve our understanding of the Earth's climate and climate change.

A proper approach to accurately calculating the Earth's entropy production rate is key to investigating the entropic properties of the Earth's climate. Calculation of the Earth's entropy production rate requires knowledge of the entropy fluxes from the Earth's incident solar radiation, from the Earth's reflected solar radiation, and from the Earth's emitted terrestrial radiation. The approaches for estimating the entropy fluxes from the reflected solar radiation and the emitted terrestrial radiation have been studied in previous papers (e.g., Stephens and O'Brien, 1993; Wu and Liu, 2010a). However, the entropy flux from the incident solar radiation has rarely been investigated, especially from the perspective of incident spectral solar irradiance.

The objective of this paper is to examine the magnitude and spectral distribution of the Earth's entropy flux from the SIM-based TOA SSI measurements from SORCE satellite. Conventionally, the Earth's entropy flux from the TOA incident solar radiation ("incident solar entropy flux" hereafter) is estimated by using a blackbody Sun's brightness temperature as proposed by Stephens and O'Brien (1993). However, the SIM-based TOA SSI measurements indicate that solar radiation does not follow the blackbody radiation law. In this paper, we take advantage of the SIM-based TOA SSI measurements to reveal the magnitude and spectral distribution of the incident solar entropy flux, to compare it with that estimated by the conventional approach, and to discuss the significance of the impact of TOA SSI variability on estimation of the incident solar entropy flux. Section 2 briefly introduces data and methodology used. Section 3 shows major results on the magnitude and spectral distribution of the incident solar entropy flux. Section 4 reveals potential causes of the difference/similarity on the estimated incident solar entropy flux. Section 5 examines the sensitivity of the incident solar entropy flux to the TOA SSI variability. Section 6 summarizes this study.

2. Data and Methodology

Daily observations of TOA SSI between 200 nm and 2400 nm have been produced through the SIM instrument on SORCE satellite since February 2003. Discussions on the SORCE SIM instrument and its product of TOA SSI data can be found in Harder et al. (2005) and Rottman et al. (2005). We use the daily SIM-based TOA SSI observations from April 2004 to October 2010 for investigating the magnitude and spectral distribution of the incident solar entropy flux. The corresponding daily TOA TSI observations from the Total Irradiance Monitor (TIM) instrument on SORCE satellite are also used as a constraint of the overall solar irradiance at the TOA.

The specific entropy intensity (L_λ, in unit of W m^{-2} K^{-1} sr^{-1} nm^{-1}) of the TOA incident solar radiation is calculated based on Planck expression, i.e.,

$$L_\lambda = \frac{2\kappa c}{\lambda^4}\left\{\left(1+\frac{\lambda^5 I_\lambda}{2hc^2}\right)\ln\left(1+\frac{\lambda^5 I_\lambda}{2hc^2}\right)-\left(\frac{\lambda^5 I_\lambda}{2hc^2}\right)\ln\left(\frac{\lambda^5 I_\lambda}{2hc^2}\right)\right\} \quad (1)$$

where h, c and κ are the Planck constant, speed of light in vacuum and the Boltzmann constant respectively, λ represents wavelength, and I_λ is the known specific energy intensity of the TOA incident solar radiation (in unit of W m^{-2} sr^{-1} nm^{-1}). Planck expression was originally formulated for calculating the specific entropy intensity of a monochromatic (blackbody) radiation beam at thermodynamic equilibrium (Planck, 1913). The applicability of Planck expression to calculating the specific entropy intensity of non-blackbody radiation at a non-equilibrium condition has been demonstrated in many previous papers (e.g., Rosen, 1954; Ore, 1955; landsberg and Tonge, 1980; Wei and Liu, 2010a).

Based on Eq. (1), we can calculate the incident solar entropy flux (J) by integrating the specific entropy intensity (L_λ) over all the wavelengths through a surface with a known zenith angle θ and solid angle Ω, that is,

$$J = \int_0^\infty d\lambda \int_\Omega L_\lambda \cos\theta d\Omega \quad (2)$$

First, the incident solar entropy flux is calculated by using Eqs. (1) and (2) under the two extreme cases: I. isotropic hemispheric incident solar radiation, i.e., the geometric factor

$\int \cos\theta d\Omega = \int_0^{2\pi} d\varphi \int_0^{\pi/2} \sin\theta \cos\theta d\theta = \pi$; II. (a) the specific solar energy intensity received at the TOA is the same as that radiated at the Sun's surface, and (b) incident solar radiation is isotropic within the cone of the solid angle to the Sun subtended by any point at the TOA. Neither of the two cases represents the reality. The former ("Assumption I" hereafter) represents the case that the space between the Earth and the Sun is full of scattering particles, and the later ("Assumption II" hereafter) represents the case that the space between the Earth and the Sun is empty. The reason we choose the two extreme cases is to test the range of the entropy flux and possible underlying assumptions.

Then, the obtained incident solar entropy flux will be compared with that estimated by the conventional approach. The conventional approach uses a blackbody Sun's brightness temperature (T_{Sun}) as presented by Stephens and O'Brien (1993), i.e.,

$$J = \frac{4}{3}\sigma T_{\text{Sun}}^3 \cos\theta_0 \frac{\Omega_0}{\pi} \tag{3}$$

where θ_0 represents globally averaged solar zenith angle, and Ω_0 represents solar solid angle to the Earth.

Finally, the sensitivity of the magnitude and spectral distribution of the incident solar entropy flux to the TOA SSI variability will be tested.

3. The incident solar entropy flux

In this section, the incident solar entropy flux by using the SIM-based TOA SSI observations and Planck expression will be first revealed. The obtained incident solar entropy flux is then compared with that by the conventional approach using a blackbody Sun's brightness temperature.

Figure 1 shows the mean SIM-based TOA SSI distribution (black solid line) based on the data collected from April 2004 to October 2010. As a comparison, the TOA SSI distribution (black dashed line) corresponding to a blackbody Sun with brightness temperature 5770 K is also shown in Figure 1. The blackbody Sun provides the TOA TSI of 1361 W m^{-2} as the mean TIM-based TOA TSI observations from April 2004 to October 2010. Similar to the findings in Harder et al. (2009, Figure 2), Figure 1 shows that the irradiance at ultraviolet (< 400 nm) wavelengths

in the SIM-based TOA SSI is much smaller in magnitude than that in the TOA SSI of the blackbody Sun, suggesting that the brightness temperature of solar radiation at ultraviolet wavelengths is much cooler than that of the blackbody Sun. On the contrary, the irradiance at visible (400 nm to 700 nm) or the near-infrared (1000 nm to 2400 nm) wavelengths in the SIM-based TOA SSI is larger than that in the TOA SSI of the blackbody Sun, reflecting that the brightness temperature of solar radiation at visible and the near-infrared wavelengths is hotter than that of the blackbody Sun. The irradiance at the near-infrared (700 nm to 1000 nm) wavelengths in the SIM-based TOA SSI looks very close to (only slightly smaller than) that in the TOA SSI of the blackbody Sun.

Next, the incident solar entropy flux is estimated. First, the specific energy intensity (I_λ) of the TOA solar radiation is estimated using known TOA SSI under Assumptions I or II. Note that, detailed discussions on the difference of the resulting specific energy (or entropy) intensity of the TOA solar radiation under the two assumptions will be presented in the next section. Then, the specific energy intensity (I_λ) corresponding to Figure 1 is used to estimate the specific entropy intensity (L_λ) based on Planck expression. Finally, the specific entropy intensity (L_λ) is integrated over the solid angle of incident solar radiation to calculate the incident solar entropy flux (shown in Figure 2).

It is noticeable that the spectral distribution of the incident solar entropy flux under the two assumptions look almost identical, except that the magnitude of the incident solar entropy flux under Assumption I is larger than that under Assumption II. The distinction of the resulting incident solar entropy flux between the two assumptions increases with wavelength. It is also evident that the estimated incident solar entropy flux exhibit remarkably similar spectral patterns to their corresponding SSI distributions as shown in Figure 1. For example, the incident solar entropy flux from the SIM-based TOA SSI shows relatively low entropy flux at ultraviolet (< 400 nm) wavelengths, relatively high entropy flux at visible (400 nm to 700 nm) and the near-infrared (1000 nm to 2400 nm) wavelengths, and slightly low entropy flux at the near-infrared (700 nm to 1000 nm) wavelengths. The overall incident solar entropy flux in the wavelength range from 200nm to 2400nm under Assumption I is equal to 1.13 W m^{-2} K^{-1} for the SIM-based TOA SSI, or 1.08 W m^{-2} K^{-1} for the blackbody Sun. The overall incident solar entropy flux within the wavelength range from 200nm to 2400nm under Assumption II is equal to 0.30 W m^{-2}

K^{-1} for both the SIM-based TOA SSI and for the blackbody Sun.

If we assume that the TOA SSI outside the wavelength range from 200nm to 2400nm corresponding to the SIM-based TOA SSI observations is equal to a constant fraction of the blackbody Sun's TOA SSI at the same wavelengths with its overall TSI being 1361 W m^{-2}, we obtain the overall incident solar entropy flux corresponding to the SIM-based TOA SSI through Planck expression of 1.24 W m^{-2} K^{-1} under Assumption I, and of 0.31 W m^{-2} K^{-1} under Assumption II. For the blackbody Sun, the estimated overall incident solar entropy flux is equal to 1.23 W m^{-2} K^{-1} under Assumption I, or 0.31 W m^{-2} K^{-1} under Assumption II. In other words, the difference between the estimated overall incident solar entropy flux based on the SIM-based TOA SSI observations and that based on the blackbody Sun is small under either of the two assumptions. The globally averaged incident solar entropy flux (i.e., one quarter of the incident solar entropy flux over a plane perpendicular to the cone of incident solar beams, see detailed derivation in the next section) is equal to 0.31 W m^{-2} K^{-1} under Assumption I for both the SIM-based TOA SSI observations and for the blackbody Sun, and 0.08 W m^{-2} K^{-1} under Assumption II for both the SIM-based TOA SSI observations and for the blackbody Sun. In other words, the globally averaged incident solar entropy flux under Assumption I is about 4 times larger than that under Assumption II, no matter whether the SIM-based TOA SSI observations or the blackbody Sun's SSI are used .

On the other hand, if using the same blackbody Sun's brightness temperature (T_{Sun} =5770 K), and assuming the globally averaged cosine of solar zenith angle $\cos\theta_0$ =0.25 and solar solid angle Ω_0 =6.77x10^{-5} sr to the planet as in Stephens and O'Brien (1993), the conventional approach yields the incident solar entropy flux of 0.08 W m^{-2} K^{-1}, about the same value as that estimated under Assumption II based on either the SIM-based TOA SSI observations or the blackbody Sun's SSI.

4. Potential causes of the difference/similarity on the estimated incident solar entropy flux

4.1. Calculation on the specific entropy intensity of the TOA incident solar radiation

As shown in Section 3, the estimated incident solar entropy flux from Assumption II or the conventional approach is significantly (4 times) lower value than that from Assumption I. Further inspection reveals that the large difference can be attributed to the difference in the

specific entropy intensity of the TOA incident solar radiation determined by the two assumptions. Also, the conventional approach [Eq. (3)] is demonstrated to match the formula of the globally averaged Earth's incident solar radiation entropy flux under Assumption II for a blackbody Sun. Details are shown in the following.

Suppose that the Sun is a blackbody with brightness temperature of T_{Sun}, the specific energy and entropy intensities at the Sun's surface can be calculated based on Planck's radiation theory (Planck, 1913),

$$I_\lambda^{\mathrm{Sun}} = \frac{2hc^2}{\lambda^5}\left\{\frac{1}{\exp\left(\frac{hc}{\lambda\kappa T_{\mathrm{Sun}}}\right)-1}\right\} \tag{4}$$

$$L_\lambda^{\mathrm{Sun}} = \frac{2\kappa c}{\lambda^4}\left\{\left(1+\frac{\lambda^5 I_\lambda^{\mathrm{Sun}}}{2hc^2}\right)\ln\left(1+\frac{\lambda^5 I_\lambda^{\mathrm{Sun}}}{2hc^2}\right)-\left(\frac{\lambda^5 I_\lambda^{\mathrm{Sun}}}{2hc^2}\right)\ln\left(\frac{\lambda^5 I_\lambda^{\mathrm{Sun}}}{2hc^2}\right)\right\} \tag{5}$$

When the solar radiation travels in space to a point with a distance r (e.g.., 1 AU) to the Sun, the specific entropy intensity of solar radiation at this point (I_λ^r) depends on the nature of how the solar radiation is received.

4.1.1. Assumption I

For Assumption I, the specific energy intensity of the TOA incident solar radiation (I_λ^r) is inversely proportional to the square of the distance (r) between the TOA and the Sun, i.e.,

$$\frac{I_\lambda^r}{I_\lambda^{\mathrm{Sun}}} = \frac{r_{\mathrm{Sun}}^2}{r^2} \tag{6}$$

where r_{Sun} represents the Sun's radius. Equation (6) indicates that the ratio of $I_\lambda^r \big/ I_\lambda^{\mathrm{Sun}}$ is a wavelength independent variable, varying only with the distance r, as demonstrated in many other references (e.g., page 18 in Goody and Yung, 1989).

Substitution of I_λ^r into Eq. (1), we obtain the corresponding specific entropy intensity as

$$L_\lambda^r = \frac{2\kappa c}{\lambda^4}\left\{\left(1+\frac{\lambda^5 I_\lambda^r}{2hc^2}\right)\ln\left(1+\frac{\lambda^5 I_\lambda^r}{2hc^2}\right)-\left(\frac{\lambda^5 I_\lambda^r}{2hc^2}\right)\ln\left(\frac{\lambda^5 I_\lambda^r}{2hc^2}\right)\right\}$$

$$= \frac{2\kappa c}{\lambda^4}\left\{\left(1+\frac{r_{\text{Sun}}^2}{r^2}\frac{\lambda^5 I_\lambda^{\text{Sun}}}{2hc^2}\right)\ln\left(1+\frac{r_{\text{Sun}}^2}{r^2}\frac{\lambda^5 I_\lambda^{\text{Sun}}}{2hc^2}\right)-\left(\frac{r_{\text{Sun}}^2}{r^2}\frac{\lambda^5 I_\lambda^{\text{Sun}}}{2hc^2}\right)\ln\left(\frac{r_{\text{Sun}}^2}{r^2}\frac{\lambda^5 I_\lambda^{\text{Sun}}}{2hc^2}\right)\right\} \quad (7)$$

Based on Eqs. (5) and (7), we get

$$\frac{L_\lambda^r}{L_\lambda^{\text{Sun}}} = \frac{\left(1+\frac{r_{\text{Sun}}^2}{r^2}\frac{\lambda^5 I_\lambda^{\text{Sun}}}{2hc^2}\right)\ln\left(1+\frac{r_{\text{Sun}}^2}{r^2}\frac{\lambda^5 I_\lambda^{\text{Sun}}}{2hc^2}\right)-\left(\frac{r_{\text{Sun}}^2}{r^2}\frac{\lambda^5 I_\lambda^{\text{Sun}}}{2hc^2}\right)\ln\left(\frac{r_{\text{Sun}}^2}{r^2}\frac{\lambda^5 I_\lambda^{\text{Sun}}}{2hc^2}\right)}{\left(1+\frac{\lambda^5 I_\lambda^{\text{Sun}}}{2hc^2}\right)\ln\left(1+\frac{\lambda^5 I_\lambda^{\text{Sun}}}{2hc^2}\right)-\left(\frac{\lambda^5 I_\lambda^{\text{Sun}}}{2hc^2}\right)\ln\left(\frac{\lambda^5 I_\lambda^{\text{Sun}}}{2hc^2}\right)} \quad (8)$$

Eq. (8) indicates that unlike the wavelength-independent ratio of the specific energy intensity at a place r (I_λ^r) and that at the Sun's surface (I_λ^{Sun}) [see Eq. (6)], the ratio of the specific entropy intensity at a place r (L_λ^r) and that at the Sun's surface (L_λ^{Sun}) varies with both wavelength λ and the distance r.

Figure 3 shows the specific energy intensity at the Sun's surface (black solid line) and that received at 1 AU scaled by $\{\max(I_\lambda^{\text{Sun}})/[2\max(I_\lambda^{1\text{AU}})]\}$ (black dashed line), for a blackbody Sun with brightness temperature 5770 K under Assumption I. Here, we use the Sun's radius of $6.96\text{x}10^8$ m and the 1AU distance to the Sun of $1.49598\text{x}10^{11}$ m. As expected, the two curves exhibit the same spectral distributions with one's amplitude being a constant fraction of the others. Both peak at the same wavelength. In fact, the 1-AU specific energy intensity is not a representative of the specific energy intensity of a blackbody Sun as discussed in previous papers (e.g., Figure 2 in Wu and Liu, 2010a).

Figure 4 shows the specific entropy intensity of solar radiation at the Sun's surface (black solid line) and that received at 1 AU scaled by $\{\max(L_\lambda^{\text{Sun}})/[2\max(L_\lambda^{1-\text{AU}})]\}$ (black dashed line), for the blackbody Sun with brightness temperature 5770 K under Assumption I as in Figure 3. Unlike the specific energy intensity at the Sun's surface and that received at 1 AU which have

the same spectral distributions, the spectral distributions of the two corresponding specific entropy intensities are different. As can be seen from Figure 4, the peak of the specific solar entropy intensity received at 1 AU slightly shifts to the right (larger wavelength) compared with that at the Sun's surface. In addition, the reduction on amplitude of the specific entropy intensity because of radiation traveling distance is wavelength dependent (shown in Figure 4).

Figure 5 further illustrates this point by plotting the ratio of specific energy intensity of solar radiation at the Sun's surface and that received at 1 AU (i.e., $I_\lambda^{\mathrm{Sun}} / I_\lambda^{\mathrm{1AU}}$), and the ratio of corresponding specific entropy intensity at the Sun's surface and that received at 1 AU (i.e., $L_\lambda^{\mathrm{Sun}} / L_\lambda^{\mathrm{1AU}}$). The former presents a constant over all the wavelengths but the latter decreases quickly with the increase of wavelength.

4.1. 2 Assumption II

For Assumption II, the specific energy intensity of solar radiation received at the TOA is the same as that radiated at the Sun's surface, i.e.,

$$I_\lambda^r = I_\lambda^{\mathrm{Sun}} \tag{9}$$

Substitution of I_λ^r into Eq. (1) leads to corresponding specific entropy intensity at the TOA (L_λ^r) as

$$L_\lambda^r = L_\lambda^{\mathrm{Sun}} \tag{10}$$

4.2 Calculation on the incident solar entropy flux

A schematic of the Sun-Earth system is shown in Figure 6. The cone of the solid angle to the Sun subtended by the cross point C of OD and the TOA is formed by its zenith angle θ and azimuth angle 2π. The spectral entropy flux (J_λ^r, W m^{-2} K^{-1} nm^{-1}) of the TOA incident solar radiation can be readily calculated by integrating the known specific entropy intensity (L_λ^r, W m^{-2} K^{-1} sr^{-1} nm^{-1}) over the solid angle to the Sun. Detailed procedures are shown in the following.

Under Assumption I, the spectral entropy flux (J_λ^r) of solar radiation received at the point C over an infinitesimal TOA area element ($d\sigma$) (i.e., perpendicular to the cone of incident solar beams) can be calculated by integrating the known specific entropy intensity received at the TOA [L_λ^r, see Eq. (7)] over a hemispheric solid angle, that is,

$$J_\lambda^r(C) = \int_{\Omega_r} L_\lambda^r \cos\theta d\Omega = \int_0^{2\pi} d\varphi \int_0^{\pi/2} L_\lambda^r \sin\theta\cos\theta d\theta = L_\lambda^r \pi \tag{11}$$

$$= \frac{2\pi\kappa c}{\lambda^4}\left\{\left(1+\frac{r_{\text{Sun}}^2}{r^2}\frac{\lambda^5 I_\lambda^{\text{Sun}}}{2hc^2}\right)\ln\left(1+\frac{r_{\text{Sun}}^2}{r^2}\frac{\lambda^5 I_\lambda^{\text{Sun}}}{2hc^2}\right)-\left(\frac{r_{\text{Sun}}^2}{r^2}\frac{\lambda^5 I_\lambda^{\text{Sun}}}{2hc^2}\right)\ln\left(\frac{r_{\text{Sun}}^2}{r^2}\frac{\lambda^5 I_\lambda^{\text{Sun}}}{2hc^2}\right)\right\} \tag{12}$$

Under Assumption II, the spectral entropy flux (J_λ^r, W m^{-2} K^{-1} nm^{-1}) of solar radiation received at the point C over an infinitesimal TOA area element ($d\sigma$) (i.e., perpendicular to the cone of incident solar beams) can be calculated by integrating the known specific entropy intensity ($L_\lambda^r = L_\lambda^{\text{Sun}}$) of the TOA incident solar radiation over the solid angle to the Sun subtended by the point C, that is,

$$J_\lambda^r(C) = \int_{\Omega_r} L_\lambda^r \cos\theta d\Omega = \int_0^{2\pi} d\varphi \int_0^{\theta} L_\lambda^{\text{Sun}} \sin\theta\cos\theta d\theta = L_\lambda^{\text{Sun}} \pi[\sin(\theta)]^2 = \frac{r_{\text{Sun}}^2}{r^2} J_\lambda^{\text{Sun}} \tag{13}$$

where

$$\sin(\theta) = \frac{r_{\text{Sun}}}{r} \tag{14}$$

$$J_\lambda^{\text{Sun}} = L_\lambda^{\text{Sun}} \pi \tag{15}$$

Notice that the solid angle in Eq. (13) is dependent on the solar radiation traveling distance r.

Now, we know the spectral entropy flux (J_λ^r, W m^{-2} K^{-1} nm^{-1}) of solar radiation received at the point C over an infinitesimal TOA area element ($d\sigma$) (i.e., perpendicular to the cone of incident solar beams). Based on this, the spectral entropy flux (J_λ^r) of solar radiation received at any given point (F) over an infinitesimal TOA area element ($d\sigma$) can be obtained by

$$J_\lambda^r(F) = J_\lambda^r(C)\cos\beta = J_\lambda^r(C)\cos(\alpha+\gamma) \tag{16}$$

where α, β, and γ represent the angles formed respectively by CD and DF, by OF and FG, and by FO and OC.

Thus, the total spectral entropy (S_λ^r, W K^{-1} nm^{-1}) of the TOA incident solar radiation can be calculated by integrating $J_\lambda^r(F)$ over the area of the TOA hemisphere facing the Sun, i.e.,

$$S_\lambda^r = \int_{\mathrm{TOA}} J_\lambda^r(F)d\sigma = \int_0^{2\pi} d\varphi \int_0^{\pi/2} J_\lambda^r(C)\cos(\alpha+\gamma) r_{\mathrm{Earth}}^2 \sin\alpha d\alpha \tag{17}$$

$$= 2\pi r_{\mathrm{Earth}}^2 J_\lambda^r(C)\int_0^{\pi/2} \cos(\alpha+\gamma)\sin\alpha d\alpha \tag{18}$$

$$\approx 2\pi r_{\mathrm{Earth}}^2 J_\lambda^r(C)\int_0^{\pi/2} \cos\alpha\sin\alpha d\alpha \tag{19}$$

$$= \pi r_{\mathrm{Earth}}^2 J_\lambda^r(C) \tag{20}$$

where the approximate equality from Eq. (18) to Eq. (19) is based on the fact that OF is approximately equal to OD and the fact that $\sin[\pi-(\alpha+\gamma)]/\mathrm{OD} = \sin\alpha/\mathrm{OF}$.

The globally averaged spectral entropy flux of the TOA incident solar radiation can then be obtained according to Eq. (20), i.e.,

$$\bar{J}_\lambda^r = \frac{S_\lambda^r}{4\pi r_{\mathrm{Earth}}^2} = \frac{J_\lambda^r(C)}{4} \tag{21}$$

Eq. (21) reveals that the globally averaged spectral entropy flux of the TOA incidnt solar radiation is equal to one quarter of the spectral entropy flux of solar radiation received over an infinitesimal TOA area element perpendicular to the cone of incident solar beams. Likewise, the globally averaged spectral energy flux of the TOA incident solar radiation equals one quarter of the spectral energy flux of solar radiation received over an infinitesimal TOA area element perpendicular to the cone of incident solar beams.

Integration of Eq. (21) over all wavelengths leads to the globally averaged incident solar entropy flux as

$$\bar{J}^r = \int_0^\infty \bar{J}_\lambda^r d\lambda = \frac{1}{4}\int_0^\infty J_\lambda^r(C)d\lambda \tag{22}$$

Substitution of Eq. (13) into Eq. (22) leads to the globally averaged incident solar entropy flux for a blackbody Sun under Assumption II as

$$\bar{J}^r = \frac{r_{\mathrm{Sun}}^2}{4r^2}\int_0^\infty J_\lambda^{\mathrm{Sun}} d\lambda = \frac{1}{4}\left(\frac{r_{\mathrm{Sun}}^2}{r^2} J^{\mathrm{Sun}}\right) = \frac{1}{4}\left[\frac{r_{\mathrm{Sun}}^2}{r^2}\left(\frac{4}{3}\sigma T_{\mathrm{Sun}}^3\right)\right] \tag{23}$$

4.3. Discussion on the conventional approach

If the globally averaged cosine of solar zenith angle is assumed as $\cos\theta_0$ =0.25 and solar solid angle to the planet equals Ω_0 =6.77x10^{-5} sr as in Stephens and O'Brien (1993), the conventional approach [Eq. (3)] can be re-written as

$$J = \frac{4}{3}\sigma T_{\text{Sun}}^3 \cos\theta_0 \frac{\Omega_0}{\pi} \tag{3}$$

$$= \left(\frac{4}{3}\sigma T_{\text{Sun}}^3\right)\frac{1}{4\pi}\left(\int_0^{2\pi} d\varphi \int_0^{\theta} \sin\theta d\theta\right) \tag{24}$$

$$\approx \left(\frac{4}{3}\sigma T_{\text{Sun}}^3\right)\frac{1}{4\pi}\left(\int_0^{2\pi} d\varphi \int_0^{\theta} \sin\theta\cos\theta d\theta\right) \tag{25}$$

$$= \left(\frac{4}{3}\sigma T_{\text{Sun}}^3\right)\frac{1}{4\pi}\left\{\pi[\sin(\theta)]^2\right\} \tag{26}$$

$$= \frac{1}{4}\left[\frac{r_{\text{Sun}}^2}{r^2}\left(\frac{4}{3}\sigma T_{\text{Sun}}^3\right)\right] \tag{27}$$

where the solar solid angle Ω_0 =6.77x10^{-5} sr to the planet in Eq. (24) has been written back as

$$\Omega_0 = \int_0^{2\pi} d\varphi \int_0^{\theta} \sin\theta d\theta \tag{28}$$

and the approximate equality from Eq. (24) to Eq. (25) is based on the fact that the solar zenith angle θ is small (or $\theta \ll 1$) so that $\cos\theta \approx 1$.

Equations (23) and (27) reveals that the conventional approach proposed by Stephens and O'Brien (1993) represents essentially the globally averaged incident solar entropy flux for a blackbody Sun under Assumption II, with the globally averaged cosine of solar zenith angle equals $\cos\theta_0$ =0.25 and solar solid angle equals Ω_0 =6.77x10^{-5} sr. This equality explains why the estimated globally averaged incident solar entropy flux from the conventional approach is about the same as that estimated under Assumption II for a blackbody Sun as shown in Section 3.

5. Sensitivity of the incident solar entropy flux to the TOA SSI variability

To further explore the sensitivity of the incident solar entropy flux to TOA SSI variability, this section uses the mean SIM-based TOA SSI distribution in the wavelength range from 200 nm to 2400 nm and constructs two additional TOA SSI scenarios in the corresponding wavelengths. The two constructed TOA SSI scenarios have the same overall solar irradiance in the wavelength range from 200nm to 2400 nm as the mean SIM-based TOA SSI. Scenario I represents the TOA SSI of a blackbody Sun. Scenario II represents the TOA SSI of a non-blackbody Sun, with the Sun's brightness temperature represented by a combination of two different half-period sinusoidal curves in the wavelength range from 200 nm to 800 nm and in the wavelength range from 801 nm to 2400 nm respectively. The spectral distribution of the incident solar entropy flux in the wavelength range from 200 nm to 2400 nm is examined using Planck expression for the three cases. The overall incident solar entropy flux within this wavelength range can be calculated by integrating the spectral distribution of the incident solar entropy flux. The obtained magnitudes and spectral distributions of the resulting incident solar entropy flux for the three cases are then compared.

Figure 7 shows the Sun's brightness temperature as a function of the wavelengths from 200 nm to 2400 nm for the three cases as described above. The black solid line represents the brightness temperature corresponding to the mean SIM-based TOA SSI distribution. The black dashed or dotted lines represent the brightness temperature corresponding to the two constructed TOA SSI scenarios. The spectral distribution of the TOA incident solar energy flux corresponding to the three cases is shown in Figure 8.

Figure 9 shows the spectral distribution of the TOA incident solar entropy flux for the three cases. Black (or gray) solid, dashed and dotted lines are results from Assumption I (or II). As can be seen, the spectral distribution of the incident solar entropy flux from both Assumptions I and II looks similar to that of the corresponding incident solar energy flux shown in Figure 8. Compared with scenario I (a blackbody Sun), the incident solar entropy flux of the SIM-based TOA SSI shows relatively low values at ultraviolet (< 400 nm) wavelengths, relatively high values at visible (400 nm to 700 nm) and the near-infrared (1000 nm to 2400 nm) wavelengths, and slightly low values at the near-infrared (700 nm to 1000 nm) wavelengths. On the other hand, the incident solar entropy flux from scenario II (a non-blackbody Sun) in general is much lower at the wavelengths less than 800 nm and much higher at the wavelengths larger than 800

nm compared with those from the other two cases, except for the wavelengths less than 280 nm where the entropy flux of the SIM-based TOA SSI is much lower than that from the others.

Based on the spectral distribution of the incident solar entropy flux in the wavelength range from 200nm to 2400 nm, we obtain the overall incident solar entropy flux within the wavelength range. For Assumption I, it is 1.13 W m^{-2} K^{-1} for the mean SIM-based TOA SSI, 1.09 W m^{-2} K^{-1} for scenario I, or 1.40 W m^{-2} K^{-1} for scenario II. In this case, the difference of the estimated overall incident solar entropy flux is up to 0.31 W m^{-2} K^{-1}, comparable to the typical value of the entropy production rate associated with the atmospheric latent heat process 0.30 W m^{-2} K^{-1} according to Peixoto et al. (1991). For Assumption II, the magnitude of the estimated overall incident solar entropy flux is much smaller than that for Assumption I.

6. Summary

The magnitude and spectral distribution of the the Earth's entropy flux from the TOA incident solar radiation (or "incident solar entropy flux") are examined by using SIM-based TOA SSI measurements from SORCE satellite. The examination is conducted under two extreme cases: I. isotropic hemispheric incident solar radiation, II. (a) the specific solar energy intensity received at the TOA is the same as that radiated at the Sun's surface, and (b) incident solar radiation is isotropic within the cone of the solid angle to the Sun subtended by any point at the TOA. The estimated incident solar entropy flux based on the SIM-based TOA SSI is further compared with that estimated by a conventional approach using a blackbody Sun's brightness temperature. The potential causes of the difference/similarity on the estimated incident solar entropy flux are revealed by examining different calculation assumptions. Finally, sensitivity experiments are performed to investigate the significance of the impact of TOA SSI variability on the estimated incident solar entropy flux.

The estimated incident solar entropy flux from the mean SIM-based TOA SSI under Assumption I exhibits 4 times larger in magnitude than that under Assumption II. The latter is about the same as that estimated by the conventional approach using a blackbody Sun's brightness temperature. It is worth emphasizing that the difference (0.31-0.08 = 0.23 W m^{-2} K^{-1}) in the estimated global averaged incident solar entropy flux between Assumptions I and II (or the conventional approach) represents about 77% of the typical entropy production rate associated

with the atmospheric latent heat process based on Peixoto et al. (1991). Also, Assumption I implies that the decrease of specific entropy intensity of solar radiation with radiation traveling distance, unlike the decrease of corresponding specific energy intensity with radiation traveling distance, is wavelength dependent. However, Assumption II represents different physics that both specific energy and entropy intensities are independent on radiation traveling distance. That explains why the estimated incident solar entropy flux is so significantly different under the two extreme assumptions. It highlights that a sound understanding on calculation of entropy flux is crucial to obtaining a correct value of the Earth's entropy production rate. A further theoretical derivation also shows that the conventional approach essentially represents the globally averaged incident solar entropy flux under Assumption II for a blackbody Sun with the globally averaged cosine of solar zenith angle being $\cos\theta_0$ =0.25 and solar solid angle to the Earth being Ω_0 =6.77x10^{-5} sr.

It is worth emphasizing that in reality the Earth's incident solar radiation does not behave as Assumptions I that requires the space is full of scattering particles. Neither does it completely as Assumption II with the necessary conditions that the space between the Earth and the Sun is empty, nothing happens to the traveling solar photons in space (i.e., no scattering, absorption, emission), and the Sun behaves as a blackbody (i.e., homogeneously emitting isotropic photons). The real situation likely operates between the conditions underlying the two extreme cases, probably relatively closer to that under Assumption II. The formulation presented here may be useful to future exploration along this line.

Furthermore, our sensitivity experiments show that even for the same overall TOA solar irradiance, the incident solar entropy flux can change significantly in both magnitude and spectral distribution with the change of TOA SSI distribution. For some case (Assumption I), the difference in magnitude of the resulting incident solar entropy flux could be larger than the typical value of the entropy production rate associated with the atmospheric latent heat process. It is also noted that although the significance of the impact of TOA SSI variability on the entropy production rate inside the Earth's climate is beyond the scope of this work, a substantial impact is possible and expected critical to determining the Earth system's thermodynamic quantities such as energy transport, temperature or humidity profiles, cloud processes. This is somewhat evident by the fact that both magnitude and spectral distribution of the incident solar entropy flux

could change significantly with TOA SSI variability. Considering that the Earth's incident solar radiation at different wavelengths reaches and warms different atmospheric layers, such a significant change on the incident solar entropy flux could possibly lead to a substantial impact on the entropy production rate generated at different Earth's atmospheric layers. Besides, the impact of TOA SSI variability on the entropy production rate of the Earth's climate comes not only from incident solar radiation but also from reflected solar radiation or even emitted terrestrial radiation, considering that the thermal structure of the Earth's climate could vary significantly with the changing TOA SSI (e.g., Cahanlan et al., 2010; Haigh et al., 2010). These results together highlight the importance and necessity of knowing the non-blackbody TOA SSI variability in calculation of the entropy production rate of the Earth's climate.

It is also noted that this study is just a start to explore the impact of TOA spectral solar irradiance on the entropy production rate of the Earth's climate. Much remains to be learned. For example, the relative agreement between the overall magnitude of the incident solar entropy flux from the mean SIM-based TOA SSI and that from a blackbody Sun with the same amount of TOA TSI (shown in Section 3) holds only true for the cases investigated here. Large discrepancy cannot be ruled out for other cases. Also, little has been known on the potential influences of TOA SSI variability on the entropy production rate generated by the processes occurring inside the Earth's climate, such as clouds and precipitation. Research along these lines is highly recommended.

Acknowledgment. This work is supported by the ESM (Earth System Modeling) through the FASTER project (www.bnl.gov/esm), and ASR (Atmospheric Science Research) programs of the U. S. Department of Energy. We thank Fabian Gans at Max-Planck-Institute for constructive comments on an early draft of this paper. We also thank Drs. Stephen E. Schwartz and Peter H. Daum at BNL for valuable discussions.

References

Cahanlan, R. F., G. Y. Wen, J. W. Harder, and P. Pilewski, 2010: Temperature responses to spectral solar variability on decadal time scales. *Geophys. Res. Lett.*, **37**, L07705, doi:10.1029/2009GL041898.

Goody, R., and Y. L. Yung, 1989: *Atmospheric Radiation: Theoretical Basis,* second edition. Oxford University Press, 519 pp.

Gray, L. J., J. Beer, M. Geller, J. D. Haigh, M. Lockwood, K. Matthes, U. Cubasch, D. Fleitmann, G. Harrison, L. Hood, J. Luterbacher, G. A. Meehl, D. Shindell, B. Van Geel, and W. White, 2010: Solar influences on climate. *Rev. Geophys.*, **48**, RG4001, doi:10.1029/2009RG000282.

Haigh, J. D., A. R. Winning, R. Toumi, and J. W. Harder, 2010: An influence of spectral solar variations on radiative forcing of climate. *Nature*, **467**, 696- 699, doi:10.1038/nature09426.

Harder, J., G. Lawrence, J. Fontenla, G. Rottman, and T. Woods, 2005: The spectral irradiance monitor: Scientific requirements, instrument design, and operation modes. *Sol. Phys.*, **230**, 141-167.

Harder, J. W., J. M. Fontenla, P. Pilewskie, E. C.Richard, and T. N. Woods, 2009: Trends in spectral solar irradiance variability in the visible and infrared. *Geophys. Res. Lett.*, **36**, L07801, doi:10.1029/2008GL036797.

Jupp, T. E., and P. M. Cox, 2010: MEP and planetary climates: insights from a two-box climate model containing atmospheric dynamics. *Phil. Trans. R. Soc. B*, **365**, 1355-1365, doi:10.1098/rstb.2009.0297.

Kleidon, A., Y. Malhi, and P. M. Cox, 2010: Maximum entropy production in environmental and ecological systems. *Phil. Trans. R. Soc. B*, **365**, 1297–1302, doi:10.1098/rstb.2010.0018.

Landsberg, P. T., and G. Tonge, 1980: Thermodynamic energy conversion efficiencies. *J. Appl. Phys.*, **51**, R1-R20.

Lean, J., 2000: Evolution of the Sun's spectral irradiance since the Maunder minimum. *Geophys. Res. Lett.*, **27**, 2425-2428.

Liu, Y., C. Liu, and D. Wang, 2011: Understanding atmospheric behaviour in terms of entropy: a review of applications of the second law of thermodynamics to meteorology. *Entropy*, **13**, 211-240; doi:10.3390/e13010211.

Lorenz, R., 2010: The two-box model of climate: limitations and applications to planetary habitability and maximum entropy production studies. *Phil. Trans. R. Soc. B*, **365**, 1349-1354, doi:10.1098/rstb.2009.0312.

Lucarini, V., and F. Ragone, 2011: Energetics of climate models: Net energy balance and meridional enthalpy transport. *Rev. Geophys.*, **49**, RG1001, doi:10.1029/2009RG000323.

Ore, A., 1955: Entropy of radiation. *Phys. Rev.*, **98**, 887-888.

Ozawa, H., S. Shimokawa, H. Sakuma, 2001: Thermodynamics of fluid turbulence: A unified approach to the maximum transport properties. *Phys. Rev. E*, **64**, 026303, doi:10.1103/PhysRevE.64.026303.

Pauluis, O., and I. M. Held, 2002a: Entropy budget of an atmosphere in radiative-convective equilibrium. Part I: Maximum work and frictional dissipation. *J. Atmos. Sci.*, **59**, 125–139.

Pauluis, O., and I. M. Held, 2002b: Entropy budget of an atmosphere in radiative-convective equilibrium. Part II: Latent heat transport and moist processes. *J. Atmos. Sci.*, **59**, 140–149.

Paltridge, G. W., G. D. Farquhar, and M. Cuntz, 2007: Maximum entropy production, cloud feedback, and climate change. *Geophys. Res. Lett.*, **34**, 1–6, L14708, doi:10.1029/2007GL029925.

Peixoto, J. P., A. H. Oort, M. De Almeida, and A. Tomé, 1991: Entropy budget of the atmosphere. *J. Geophys. Res.*, **96**, 10,981–10,988, doi:10.1029/91JD00721.

Planck, M., 1913: *The Theory of Heat Radiation*, 224 pp. (English translation by Morton Mausius (1914), Dover Publications, New York, 1959).

Pujol, T., and J. Fort, 2002: States of maximum entropy production in a one-dimensional vertical model with convective adjustment. *Tellus*, **54A**, 363–369.

Rosen, P., 1954: Entropy of radiation. *Phys. Rev.*, **96**, 555.

Rottman, G., J. Harder, J. Fontenla, T. N. Woods, O. R. White, and G. Lawrence, 2005: The Spectral Irradiance Monitor (SIM): Early observations. *Sol. Phys.*, **230**, 205-224.

Stephens, G. L., and D. M. O'Brien, 1993: Entropy and climate, I, ERBE observations of the entropy production. *Q. J. R. Meteorol. Soc.*, **119**, 121–152.

Wang, B, T. Nakajima, G. Shi, 2008: Cloud and Water Vapor Feedbacks in a Vertical Energy-Balance Model with Maximum Entropy Production. *J. Clim.*, **21**, 6689-6697, doi: 10.1175/2008JCLI2349.1.

Wu, W., and Y. Liu, 2010a: Radiation entropy flux and entropy production of the Earth system. *Rev. Geophys.*, **48**, RG2003, doi:10.1029/2008RG000275.

Wu, W., and Y. Liu, 2010b: A new one-dimensional radiative equilibrium model for investigating atmospheric radiation entropy flux, *Phil. Trans. R. Soc. B*, **365**, 1367–1376, doi:10.1098/rstb.2009.0301.

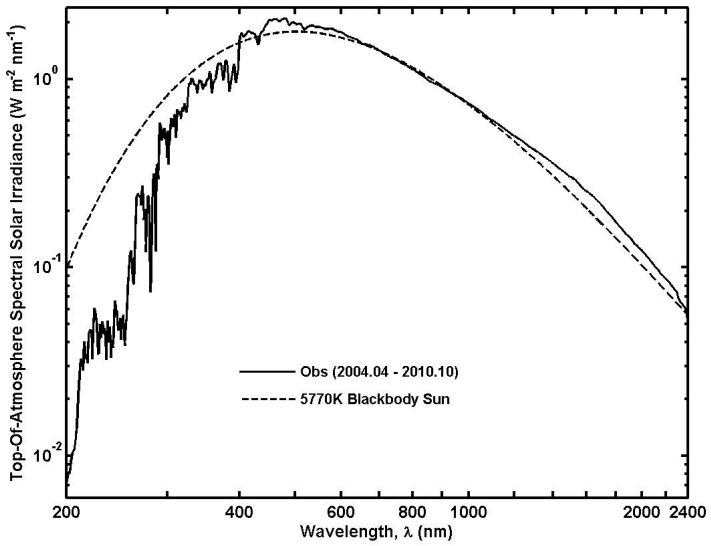

Figure 1. Black solid line represents the mean SIM-based TOA SSI distribution based on the data collected from April 2004 to October 2010. Black dashed line represents the TOA SSI distribution corresponding to a blackbody Sun with brightness temperature 5770 K.

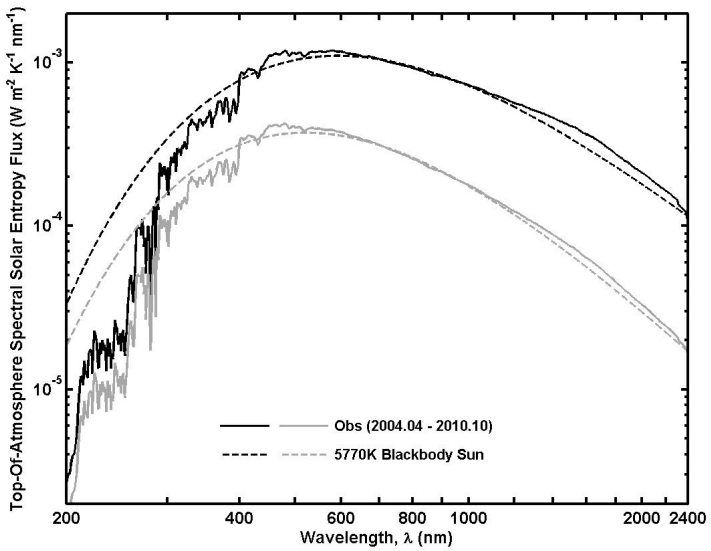

Figure 2. The spectral distribution of the incident solar entropy flux corresponding to the TOA SSIs as shown in Figure 1. Black solid and dashed lines are calculated under Assumption I. Gray solid and dashed lines are calculated under Assumption II.

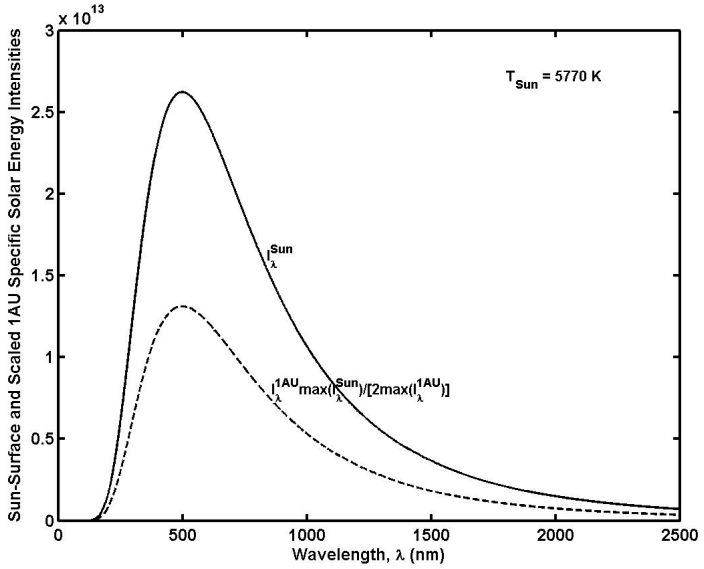

Figure 3. Specific energy intensity of solar radiation at the Sun's surface (black solid line) and that received at 1 AU scaled by $\{\max(I_\lambda^{Sun})/[2\max(I_\lambda^{1AU})]\}$ (black dashed line), for a blackbody Sun with brightness temperature 5770 K under Assumption I.

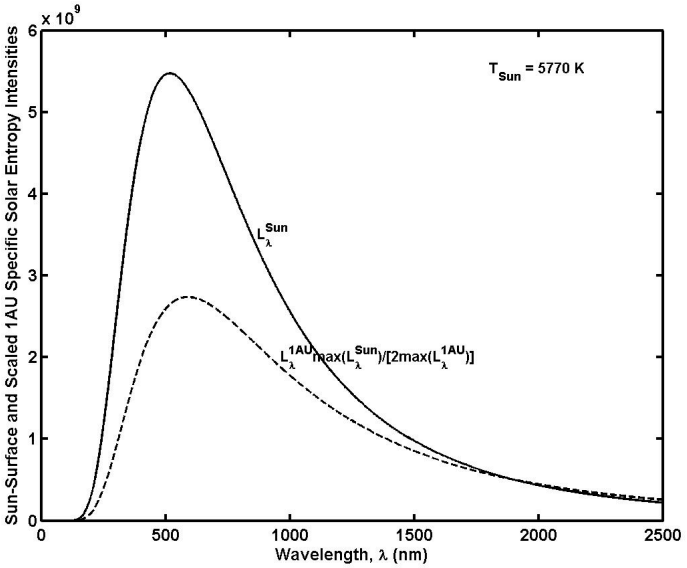

Figure 4. Specific entropy intensity of solar radiation at the Sun's surface (black solid line) and that received at 1 AU scaled by $\{\max(L_\lambda^{Sun})/[2\max(L_\lambda^{1AU})]\}$ (black dashed line), for a blackbody Sun with brightness temperature 5770 K under Assumption I.

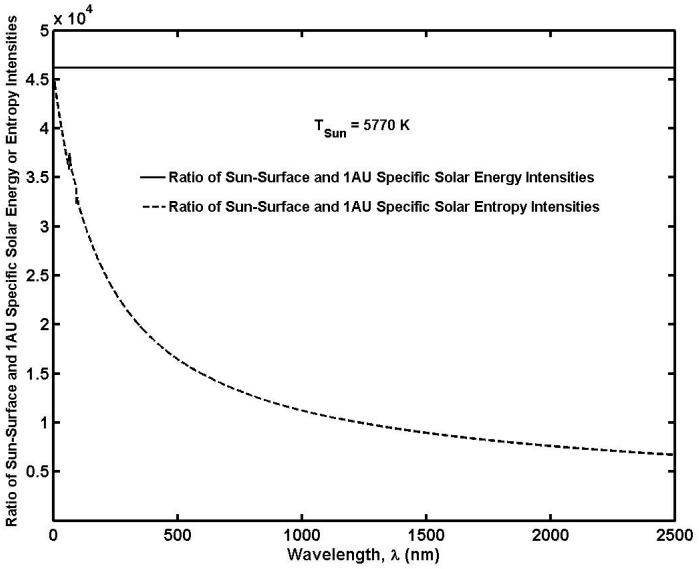

Figure 5. Black solid line: the ratio of specific energy intensity of solar radiation at the Sun's surface and that received at 1 AU, for a blackbody Sun with brightness temperature 5770 K under Assumption I. Black dashed line: the ratio of corresponding specific entropy intensity at the Sun's surface and that received at 1 AU for the same blackbody Sun.

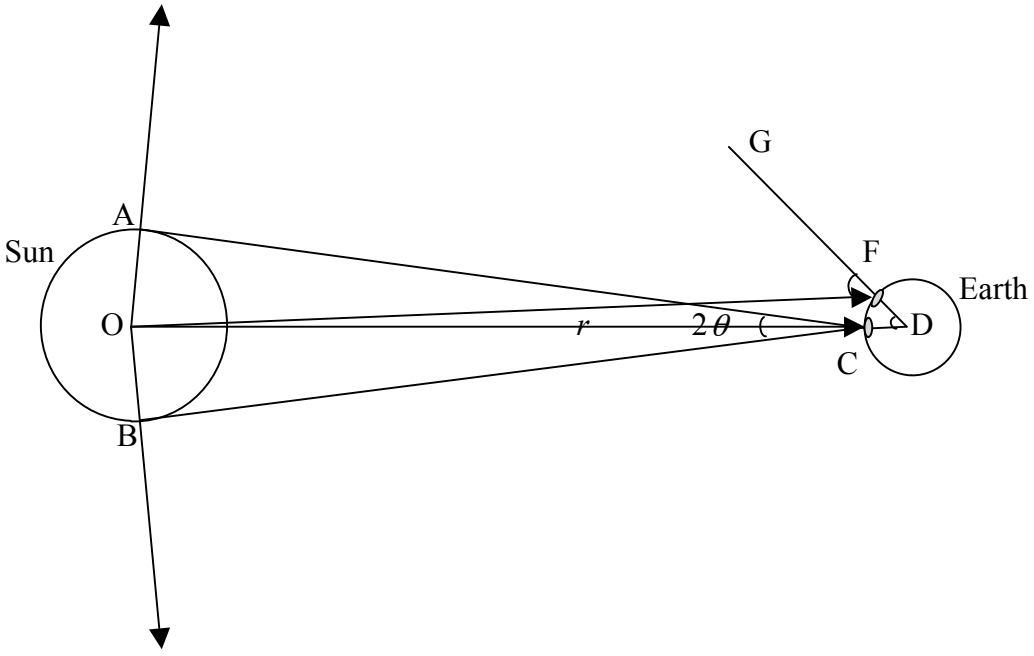

Figure 6. A schematic of the Sun-Earth system. O represents the center of the Sun and D represents the center of the Earth. Both AC and BC are tangent to the Sun's surface at A and B respectively. C is the cross point of OD and the TOA. F is the cross point of DG and the TOA. r represents the distance (i.e., 1 AU) between the Sun and the Earth. 2θ represents the acute angle formed by BC and AC.

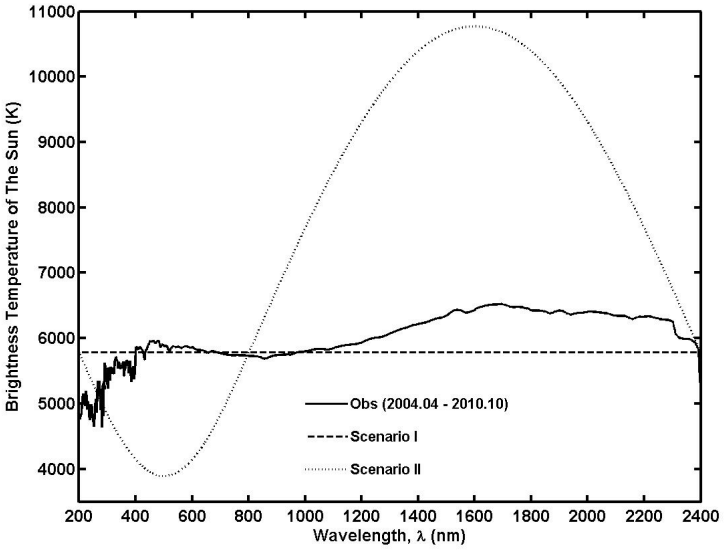

Figure 7. The Sun's brightness temperature as a function of the wavelengths from 200 nm to 2400 nm for the three cases. Black solid line: brightness temperature corresponding to the mean SIM-based SSI from April 2004 to October 2010. Black dashed or dotted lines: brightness temperatures corresponding to the two constructed TOA SSI scenarios with the same overall solar irradiance in the wavelength range from 200nm to 2400 nm as that from the mean SIM-based TOA SSI.

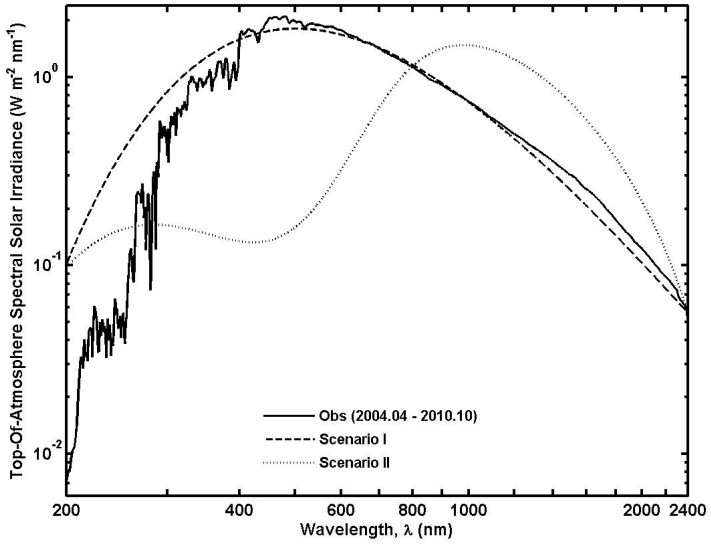

Figure 8. The spectral distribution of the energy flux from the TOA incident solar radiation for the three cases as shown in Figure 7.

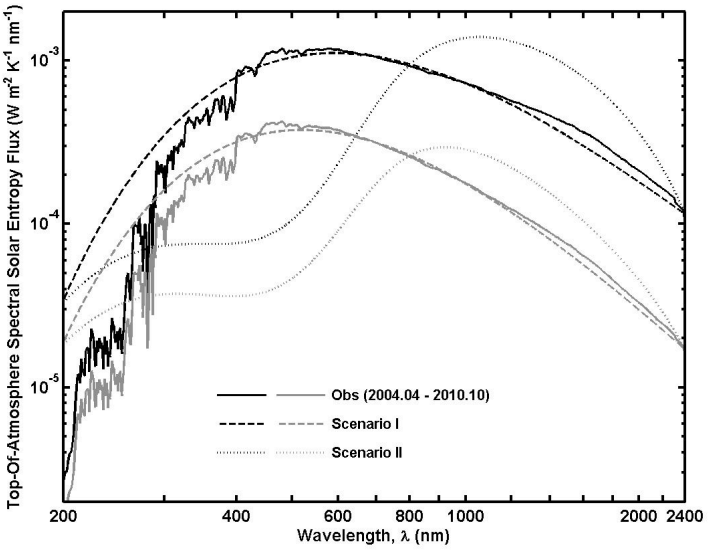

Figure 9. The spectral distribution of the entropy flux from the TOA incident solar radiation for the three cases as shown in Figure 7 or Figure 8. Black (or gray) solid, dashed and dotted lines are calculated under Assumption I (or II).